Supplement of Geosci. Model Dev., 10, 827–841, 2017
http://www.geosci-model-dev.net/10/827/2017/
doi:10.5194/gmd-10-827-2017-supplement

Geoscientific Model Development
Open Access
EGU

Supplement of

OZO v.1.0: software for solving a generalised omega equation and the Zwack–Okossi height tendency equation using WRF model output

Mika Rantanen et al.

Correspondence to: Mika Rantanen (mika.p.rantanen@helsinki.fi)

S1 Supplementary material

S1.1 Forcing terms

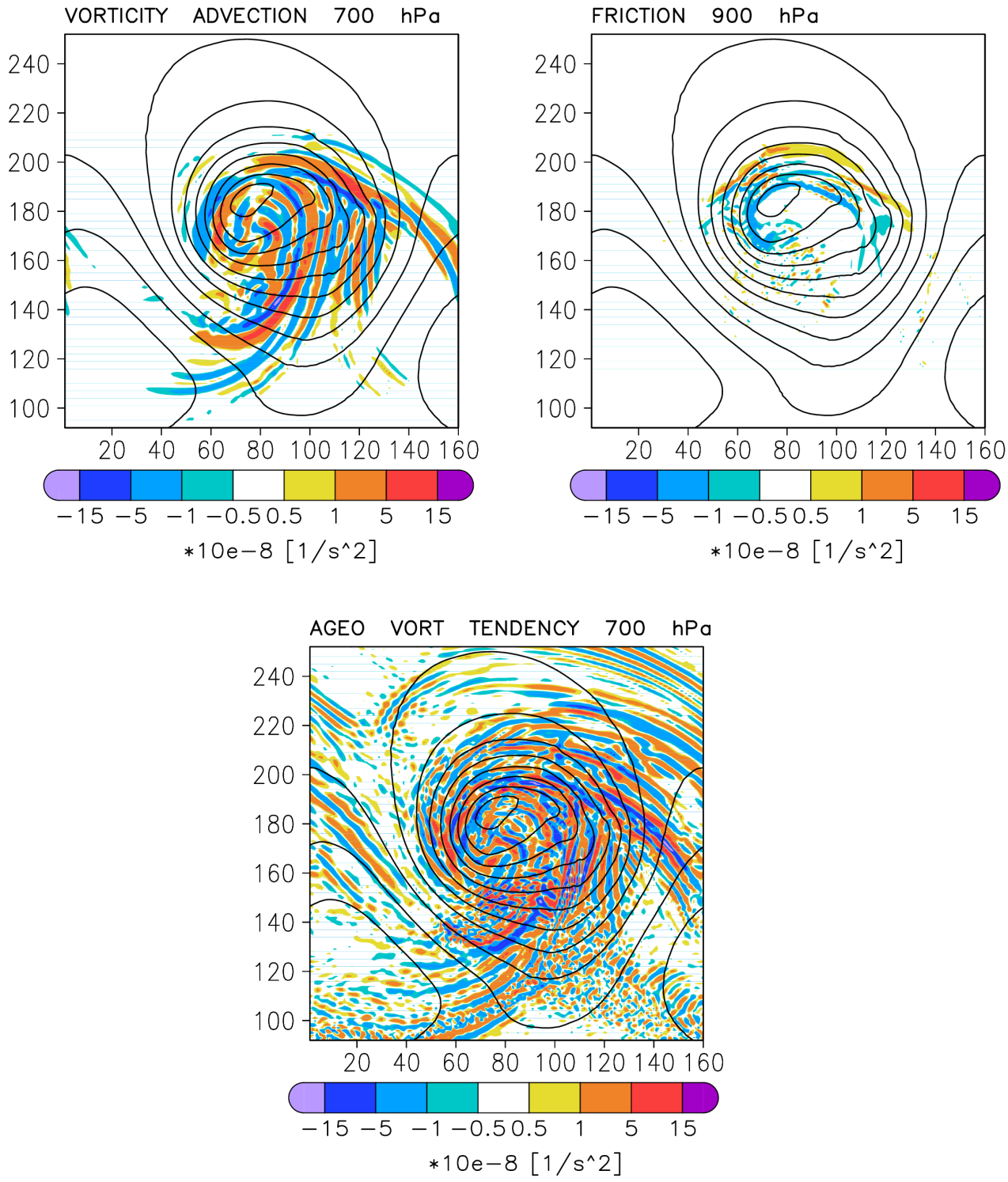

Figure S1: Vorticity advection ($-\mathbf{V} \cdot \nabla(\zeta + f)$), friction ($\mathbf{k} \cdot \nabla \times \mathbf{F}$) and ageostrophic vorticity tendency ($\partial \zeta ag / \partial t$). Note that friction is at the 900 hPa level but vorticity advection and ageostrophic vorticity tendency at 700 hPa.

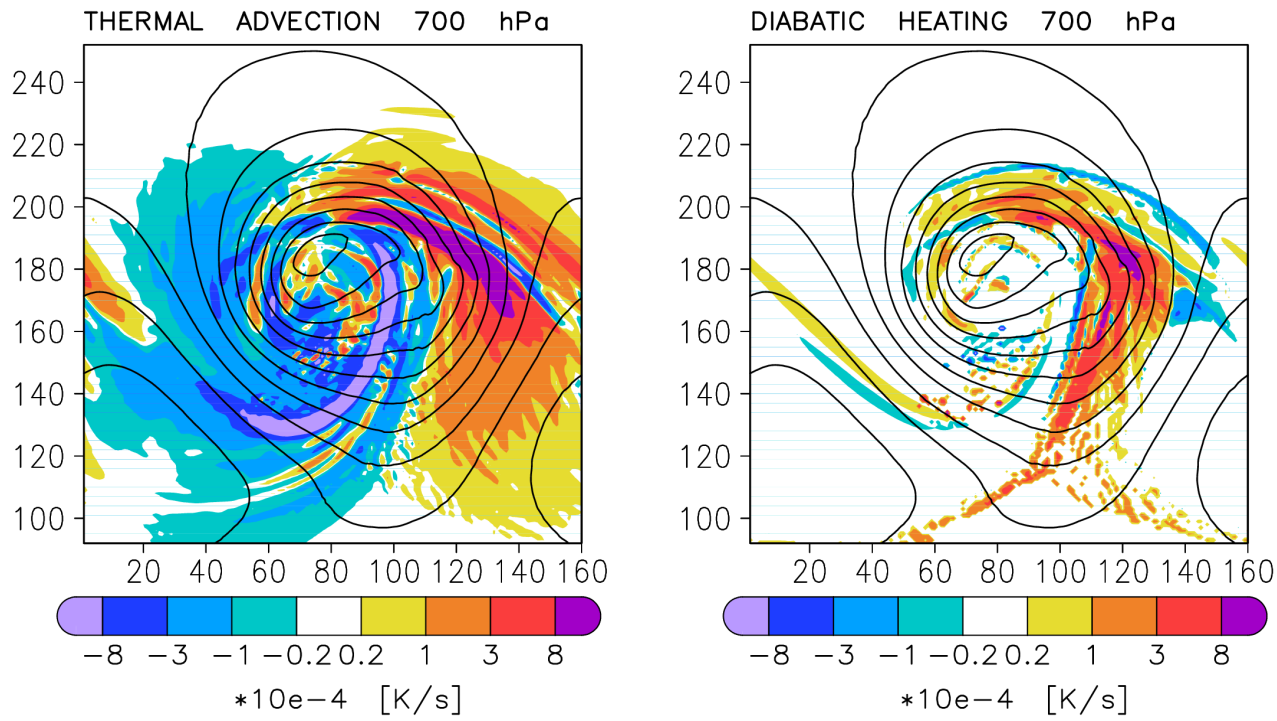

Figure S2: Thermal advection ($-\mathbf{V} \cdot \nabla T$) and diabatic heating ($Q$) at the 700 hPa level.

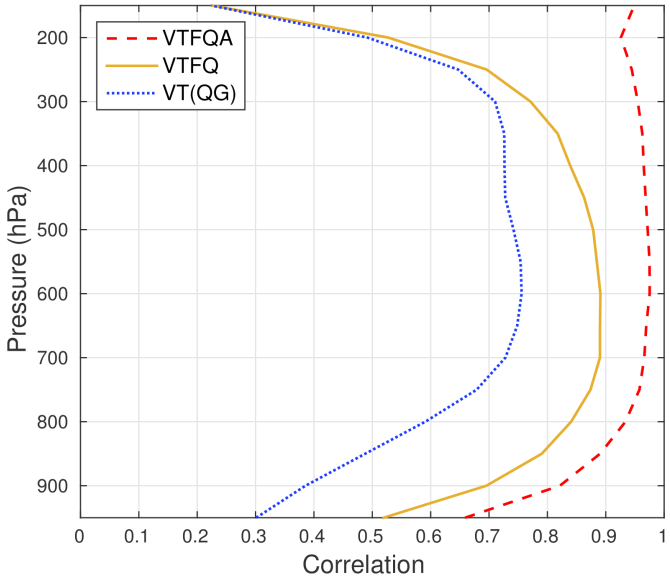

Figure S3: Correlation of the omega equation solutions with ω_{WRF} at 100 km grid spacing. $VTFQA = \omega_{TOT}$, $VTFQ = \omega_{TOT} - \omega_A$, $VT(QG) = \omega_{V(QG)} + \omega_{T(QG)}$.

S1.2 Results at 100 km horizontal resolution

Figures S3, S4 and S5 provide information on correlations and RMS values of vertical motions and height tendencies diagnosed with OZO from a 100 km horizontal resolution WRF simulation. The correlations for vertical motion (lines $VTFQA$, $VTFQ$ and $VT(QG)$ in Fig. S3 and Fig. 3) are slightly but systematically better at 100 km than at 25 km resolution. Higher resolution brings much more mesoscale detail in the simulated weather system, which tends to increase the discrepancy between ω_{TOT} and ω_{WRF}, and thus reduce the correlation between the fields. These mesoscale features also increase the magnitude of the imbalance term and the other terms omitted in the quasi-geostrophic omega equation, thus deteriorating the correlation for the quasi-geostrophic solution at higher resolution.

As expected, the RMS amplitude of vertical motions is smaller at 100 km than 25 km resolution. In addition, there are some differences in the relative importance of the individual ω components. RMS(ω_T) increases more than RMS(ω_V) when the horizontal resolution is improved (see Section 6.2). The effect of latent heat release has also

tendency to increase at higher resolution (Willison et al., 2013) and our results confirm that vertical motions induced by diabatic heating are strongly sensitive to the horizontal resolution, especially in the lower troposphere where shallow convection occurs (compare Fig. S4 to Fig. 4). In the lower troposphere, in particular, the imbalance term is also much larger at 25 km than 100 km resolution.

Figures S5 and 7 show that the error in height tendency fields grows as well when the resolution is improved, but this only leads to a marginal deterioration in the tropospheric correlation between the calculated and directly diagnosed height tendencies.

Figures S6, S7, S8 and S9 show the horizontal distributions of the diagnozed vertical motions and height tendencies at 100 km resolution, analogously to the corresponding results for the 25 km simulation in Figs. 1, 5, 6 and 8. The basic features are largely the same but, as expected, there is much less small-scale detail in the results derived from the 100 km simulation.

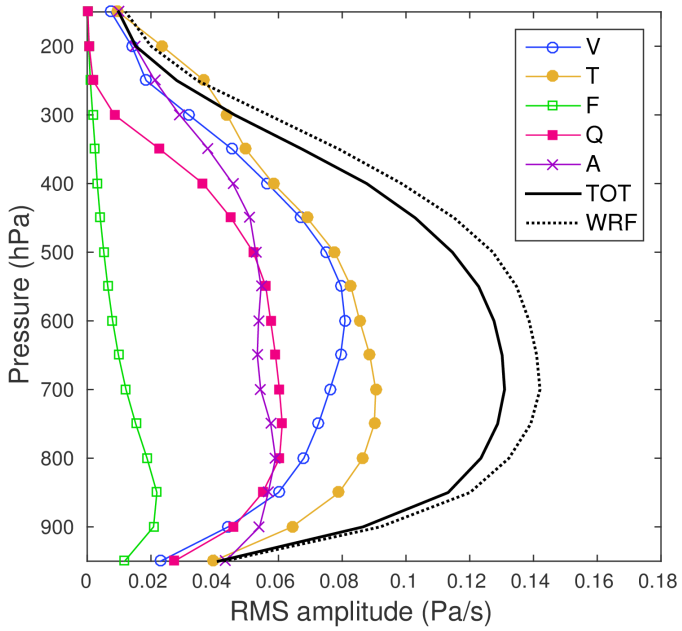

Figure S4: RMS amplitudes of ω_{WRF}, ω_{TOT}, and the individual ω components from Eq. 5 at 100 km grid spacing.

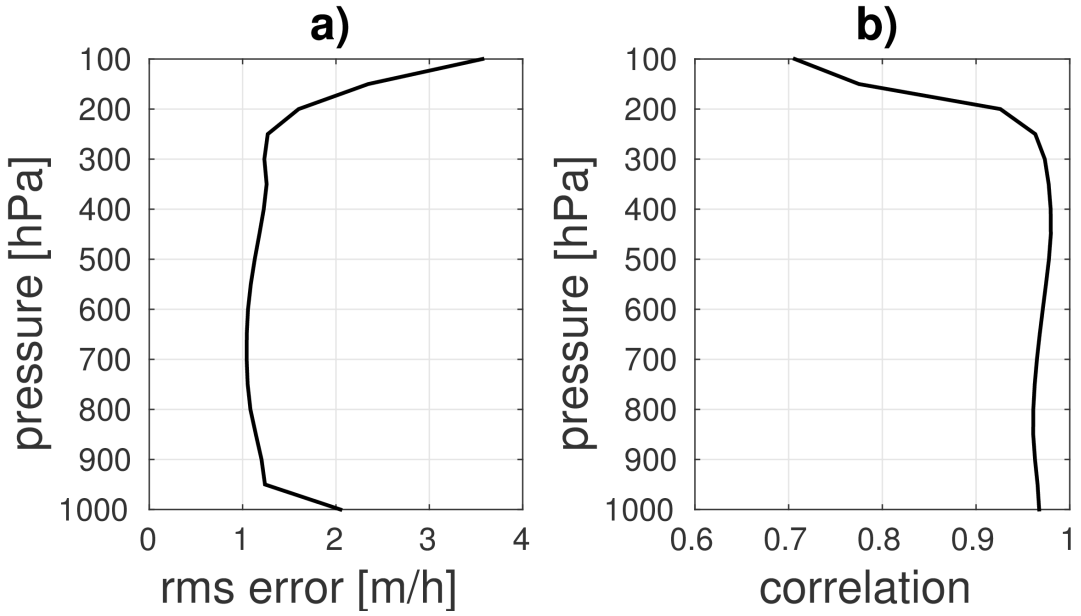

Figure S5: Time mean a) rms error and b) spatial correlation coefficient between calculated and WRF height tendency over the last 8 days of the 10-day simulation at 100 km grid spacing.

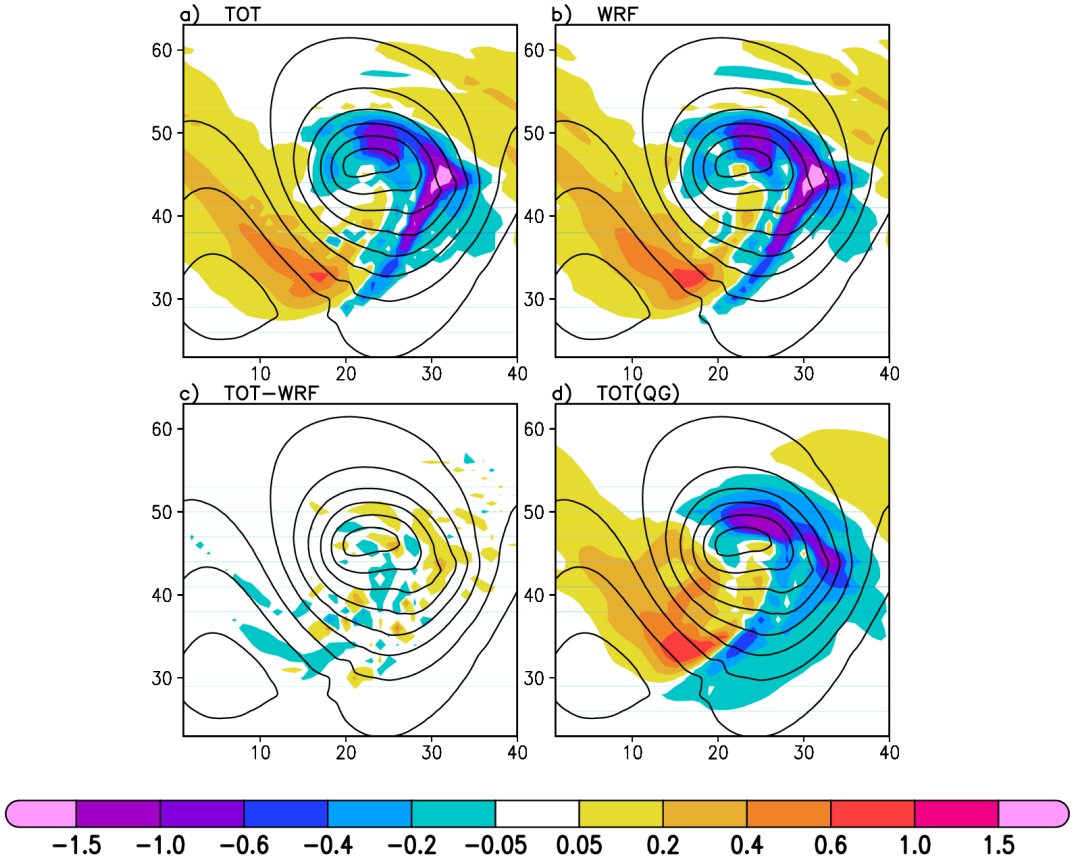

Figure S6: a) The sum of all ω components from Eq. (5) (ω_{TOT}), b) ω from WRF (ω_{WRF}), c) difference ($\omega_{TOT} - \omega_{WRF}$) and d) solution of the QG omega equation ($\omega_{V(QG)} + \omega_{T(QG)}$) at 700 hPa level at time 118 h, using 100 km grid spacing. Unit is $Pa\,s^{-1}$. Contours show geopotential height at 900 hPa level with an interval of 50 m. Labels on x- and y-axes indicate grid point numbers. Note that the area covers only half of the model domain in the meridional direction. Compare with Fig. 1 in the main paper.

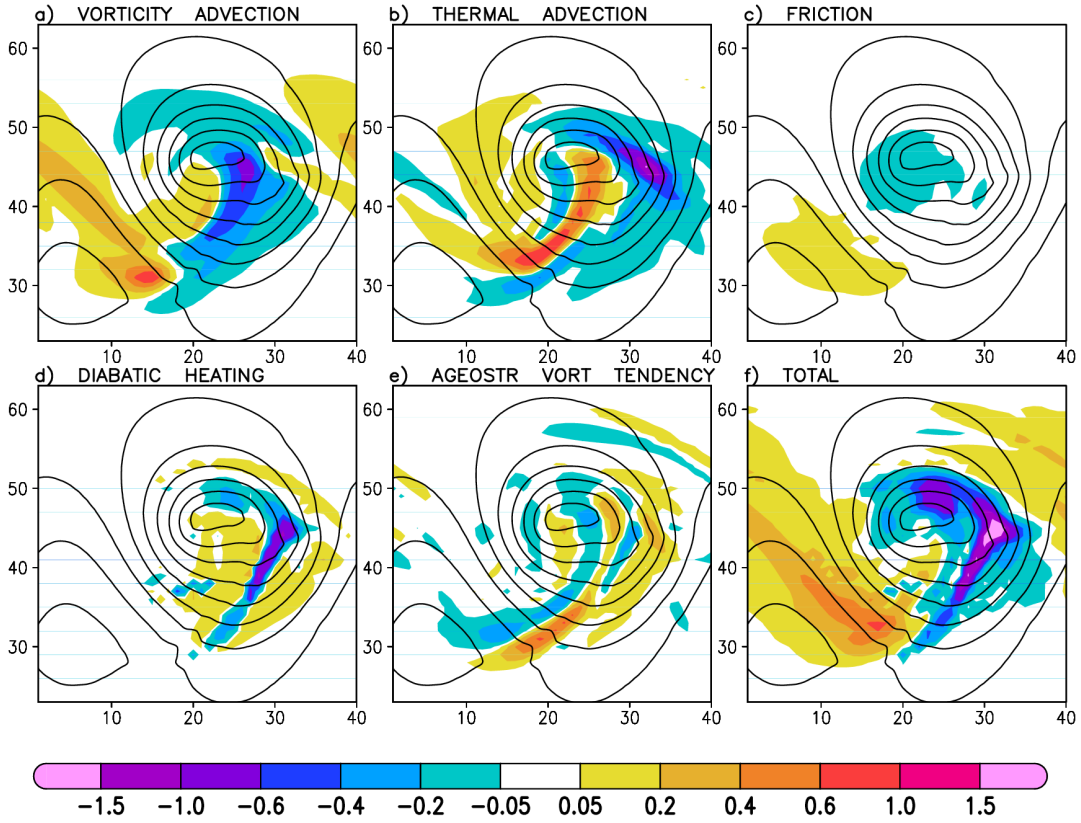

Figure S7: Vertical motions induced by individual forcing terms at level 700 hPa at time 118 h, using 100 km grid spacing. a) ω_V, b) ω_T, c) ω_F, d) ω_Q, e) ω_A and f) ω_{TOT}. Unit is $Pa\,s^{-1}$ and contour lines show 900 hPa geopotential height with 50 m interval. Compare with Fig. 5 in the main paper.

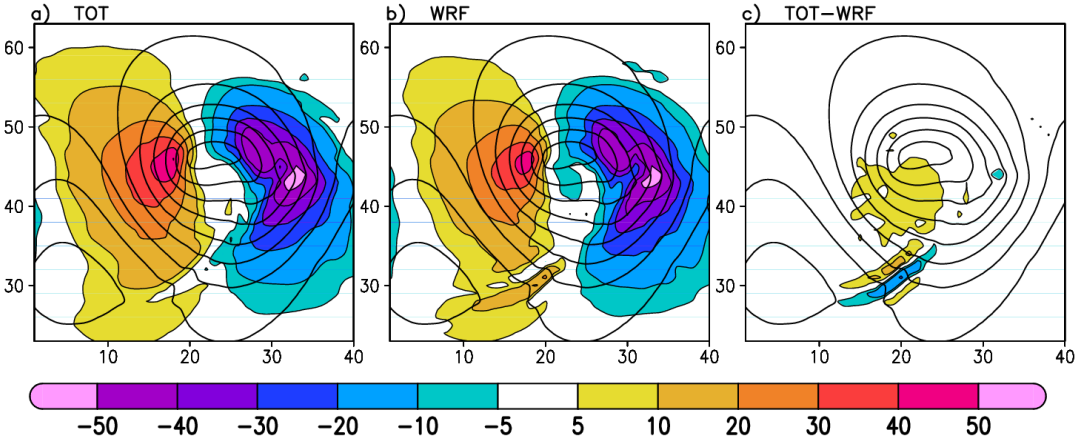

Figure S8: As Fig. S6, but for the height tendency at 900 hPa. Unit is $m\,h^{-1}$. Compare with Fig. 6 in the main paper.

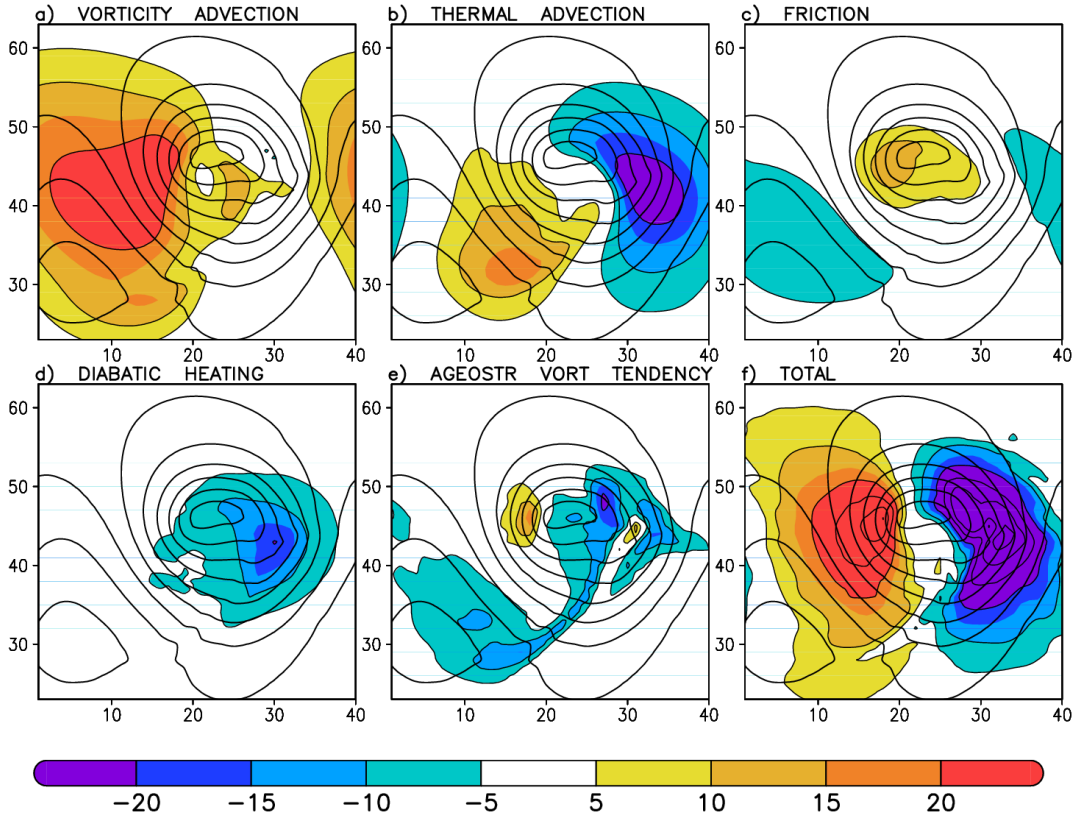

Figure S9: As Fig. S7, but for height tendency components at 900 hPa level. Unit is $m\,h^{-1}$. Note that the color scale of f) differs from Fig. S8a. Compare with Fig. 8 in the main paper.

References

Willison, J., Robinson, W. A., and Lackmann, G. M.: The importance of resolving mesoscale latent heating in the North Atlantic storm track, J. Atmos. Sci., 70, 2234–2250, 2013.